AIP ADVANCES **4**, 017131 (2014)

Energy transport in crystalline DNA composites

Zaoli Xu, Shen Xu, Xiaoduan Tang, and Xinwei Wang[a]
Department of Mechanical Engineering, 2010 Black Engineering Building Iowa State University, Ames, IA 50011, USA

(Received 26 November 2013; accepted 21 January 2014; published online 29 January 2014)

This work reports on the synthesis of crystalline DNA-composited films and microfibers, and details the study of thermal energy transport in them. The transient electro-thermal technique is used to characterize the thermal transport in DNA composite microfibers, and the photothermal technique is used to explore the thermal transport in the thickness direction of DNA films. Compared with microfibers, the DNA films are found to have a higher thermal transport capacity, largely due to the carefully controlled crystallization process in film synthesis. In high NaCl concentration solutions, the bond of the Na^+ ion and phosphate group aligns the DNA molecules with the NaCl crystal structure during crystallization. This results in significant enhancement of thermal transport in the DNA films with aligned structure. [http://dx.doi.org/10.1063/1.4863924]

I. INTRODUCTION

DNA plays a vital role as the carrier of biological information for its base sequences. DNA has recently seen an increase in interest as a promising molecular material due to its ease of surface modification and self-assembly capabilities. These make it accessible to construct nanostructures, such as nanoparticles, nanocrystals, nanowires, and molecular circuits.[1–3] DNA was first suggested to be an electrical conductor soon after the discovery of its double helix structure.[4] The studies of electrical conduction of DNA have been revived in the 1990s, since the electron transfer reactions along DNA chains are found to be important in radiation damage and repair.[5] Studies have also shown that the electric properties of DNA are versatile.[6] Over distances of a few nanometers, there is an agreement that the electrons can transfer along the DNA chain bases by coherent quantum tunneling and diffusive thermal hopping.[7–10] However, everything from insulating to superconducting behavior of long-range electron transfer through DNA has all been reported.[11–16] Thus, the electrical conductivity of DNA is believed to depend on various factors, such as length, base sequences, and ambient conditions.

As an important aspect of the conduction mechanism, thermal conduction within DNA still remains poorly understood. Only a few have recently began to study the thermal conduction in DNA. The thermal conductivity of a DNA-gold composite has been measured to be 150 W/m · K,[17] comparable to 317 W/m · K for the thermal conductivity of pure gold at 300 K.[18] In contrast, a Peyrard-Bishop-Dauxois (PBD) modeling result suggests that the thermal conductivity of the DNA double helix is 1.8×10^{-3} W/m · K,[19] and a 3-D coarse-grained modeling estimates that the thermal conductivity of a uniform (polyG-polyC) DNA is no more than 0.3 W/m · K.[20] Both modeling results indicate that the DNA molecule is a poor heat conductor with a low thermal conductivity. However, it is still a mystery whether the DNA molecule is a good heat conductor or insulator experimentally, as is the thermal conduction mechanism along DNA chain bases, which needs to be figured out entirely.

[a]Corresponding author. Tel: 515-294-8023; Email: xwang3@iastate.edu

Thermal properties of DNA are shown to alter significantly as it denatures.[19] The double-stranded structure of DNA can unravel into two single strands and denaturate, which is important for its relationship to DNA transcription. The denaturation of DNA via thermal fluctuations is thought to play a major role in the formation of the transcription bubble. The detailed information on the dynamics of the thermal fluctuations and their interaction along the strand are encoded by the alteration of thermal properties of DNA. However, the modeling results do not have a consistent conclusion at present. The PBD model predicts a substantial increase in the thermal conductance upon DNA denaturation, while another nonlinear model shows a drop in the thermal conductance. Thus, understanding of the thermal conduction of DNA is also important to clarify the denaturation mechanism.

Metal coatings will have a large thermal effect on the overall thermal transport in metalized DNA, like the DNA-gold composite, due to their high thermal conductivities. As a result, the thermal properties of pure DNA molecules still remain unclear. If a DNA molecule can be composited with a low thermal conductivity material, it may be possible to estimate the thermal properties of DNA from this composite. DNA is commonly kept in Tris-EDTA (TE) buffer solution to keep it from degeneration. As a result, we have come up with a method to qualitatively estimate the thermal properties of DNA molecule by measuring the composites formed from the DNA-TE buffer solution. In particular, the thermal properties of DNA-composited fibers and films are successfully characterized to give a pioneering insight into the thermal transport along DNA molecules.

This work is organized as follows. We begin with the preparations of samples for the experiment. Then the thermal characterization technologies are introduced for characterizing the thermal properties of DNA fibers and films respectively. The results for the composites formed from the DNA-TE buffer solutions with two different DNA concentrations are reported. The results for the fibers and films are compared for data processing and discussion.

II. Materials and Methods

A. Sample Preparation

Preparation of DNA-TE buffer solution: DNA from salmon testes (∼2 kbp, Sigma-Aldrich) and sodium chloride (NaCl) are dissolved in TE buffer (10 mM Tris-HCl and 1.0 mM EDTA). We cannot draw fibers out of the solution without dissolving them, so NaCl is added to the solution for that purpose. Two concentrations of the solutions are used: one is 0.5 wt% DNA with 5 wt% NaCl, and the other is 1 wt% DNA with 1 wt% NaCl. The latter solution is denser than the former one due to the higher concentration of DNA. The prepared DNA-TE buffer solutions are stored in a freezer at -20°C and thawed each time before use.

Synthesis of DNA-composited fibers from DNA-TE buffer solution: The method for direct drawing of suspended fibers from liquid polymers[21] is adopted and modified in this work for making suspended DNA-composited fibers, as illustrated in Fig. 1. The DNA-TE buffer solution is first transferred and dropped onto two copper electrodes by using a syringe [Fig. 1(a)]. When the solution reaches consistency through evaporation, a tungsten tip (with a tip diameter of 25 μm) is dipped into one droplet by any available angle, and the fiber can be most readily hand-drawn out at the edge of the droplet, as shown in Fig. 1(b). The drawn fiber will be attached to the second droplet and then dissolve from the tip [Fig. 1(c)]. The entire fiber continues to dry to form a suspended solid fiber [Fig. 1(d)]. The length and diameter of the fiber are evaluated under a scanning electron microscope (SEM) [Fig. 1(e)]. The length is largely determined by the pre-set gap distance and the direction of the drawing process with respect to the electrode edges. In contrast, the fiber diameter is not well-controlled. Although it is believed that the fiber diameter increases with the solution viscosity when the solution dries,[21] the current fiber drawing process is unable to produce fibers out of the solution repeatedly with a similar solution viscosity, even with the same solution concentration. As listed in Table I, the fiber diameter varies from sample to sample. Nevertheless, a typical drawn fiber is observed round and uniform over the whole length.

Synthesis of DNA-composited films from DNA-TE buffer solution: Figure 2 shows the fabrication processes to make DNA-composited films from the solution. The thickness is a quite important

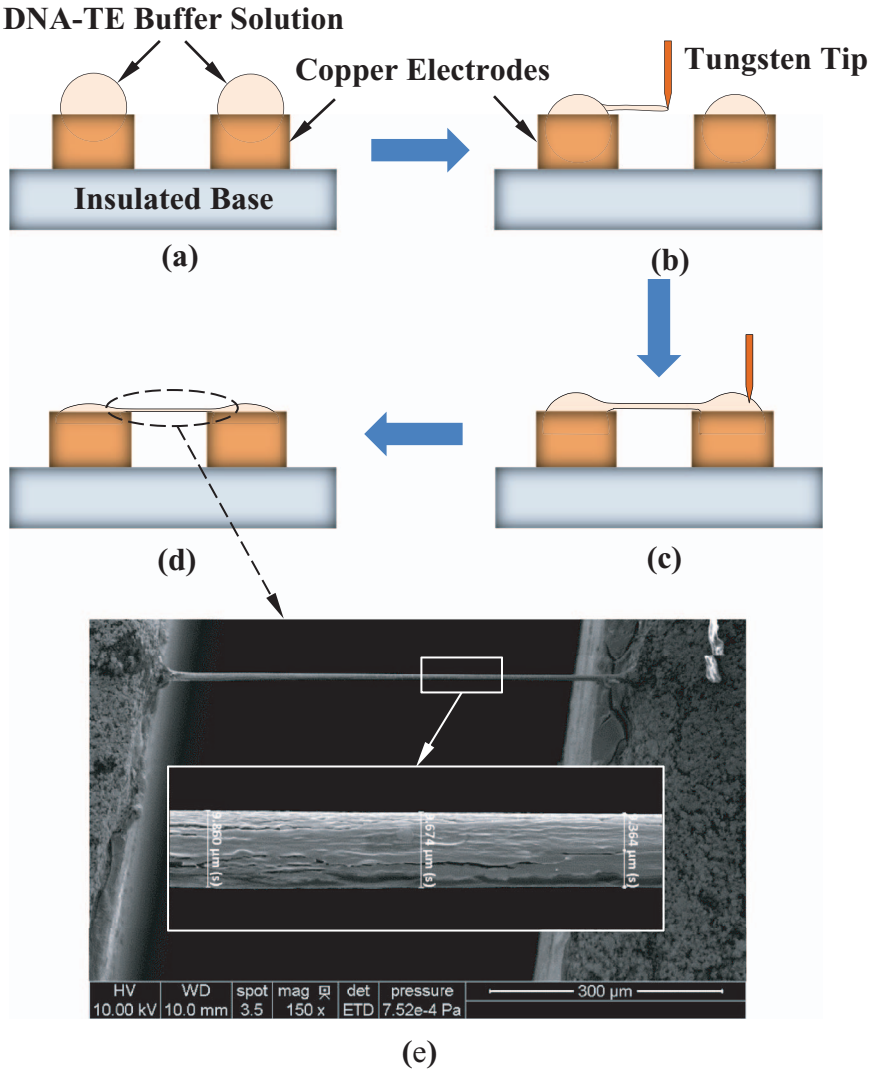

FIG. 1. The fabrication method for forming a suspended DNA-composited fiber from DNA-TE buffer solution. (a) The solution is first transferred and dropped onto two disconnected electrodes. (b) When the solution reaches consistency through evaporation, a tungsten tip (with a diameter of 25 μm) is dipped into the droplet on the left electrode, and the fiber can be most easily hand-drawn out at the edge of the droplet. (c) The fiber would be attached to the droplet on the right electrode, and then dissolved from the tip. (d) The entire fiber continues to dry to form a suspended solid fiber. (e) SEM image of a well-formed DNA-composited fiber drawn from the DNA-TE buffer solution with 0.5 wt% DNA and 5 wt% NaCl.

parameter in determining thermal conductivity and heat capacity of a film. However, a major challenge during the fabrication is that the film is not uniform in the thickness direction due to the growth of large NaCl crystal structures. Therefore, the following steps are developed, when necessary, to form a uniform film. The solution is first dropped inside a washer taped to a microscope slide. The slide with the solution is then spun in a spin coater to make the droplet uniform in the lateral direction [Fig. 2(a)]. Second, the droplet is frozen at a low temperature (-20°C) for several minutes and then the washer is taken off, and continues to be frozen for 1 hour [Fig. 2(b)]. Then the moisture is removed through the process of sublimation by placing the frozen sample in a vacuum chamber down to 100 mTorr for another hour [Fig. 2(c)]. Large NaCl crystal structures can sometimes still be observed by naked eyes on part of the film, but only the most uniform regions are chosen for thermal characterization, as shown in Fig. 2(d). The above measures are taken to improve the uniformity

TABLE I. Experimental data and calculated results for all DNA-composited fibers.

Fibers	L (mm)	D (μm)	$\alpha_{real+rad+gold}$ (10^{-7}m^2/s)	α_{real} (10^{-7}m^2/s)	k_{real} (W/m $\cdot$ K)
Group 1_1	0.447	8.32	6.33 $\pm$ 0.63	4.67 $\pm$ 0.63	0.76 $\pm$ 0.10
Group 1_2	0.613	6.42	7.17 $\pm$ 0.06	5.15 $\pm$ 0.06	0.84 $\pm$ 0.01
Group 1_3	0.778	3.84	6.11 $\pm$ 0.12	2.97 $\pm$ 0.12	0.48 $\pm$ 0.02
Group 1_4	0.56	3.19	10.13 $\pm$ 0.11	5.48 $\pm$ 0.11	0.89 $\pm$ 0.02
Group 1_5	0.448	5.50	3.97 $\pm$ 0.01	2.26 $\pm$ 0.01	0.37 $\pm$ 0.00
Group 1_6	0.621	3.90	8.39 $\pm$ 0.14	5.19 $\pm$ 0.14	0.85 $\pm$ 0.02
Group 1_7	0.536	5.58	6.17 $\pm$ 0.17	2.94 $\pm$ 0.17	0.48 $\pm$ 0.03
Group 1_8	0.648	7.34	4.14 $\pm$ 0.09	2.19 $\pm$ 0.09	0.36 $\pm$ 0.01
Group 2_1	1.115	15.16	4.17 $\pm$ 0.08	1.92 $\pm$ 0.08	0.33 $\pm$ 0.01
Group 2_2	0.397	1.31	10.31 $\pm$ 0.19	1.94 $\pm$ 0.19	0.33 $\pm$ 0.03
Group 2_3	0.515	8.39	2.76 $\pm$ 0.03	1.42 $\pm$ 0.03	0.24 $\pm$ 0.01
Group 2_4	0.435	5.27	4.82 $\pm$ 0.07	2.69 $\pm$ 0.07	0.46 $\pm$ 0.01
Group 2_5	0.534	8.24	3.13 $\pm$ 0.04	1.62 $\pm$ 0.04	0.28 $\pm$ 0.01

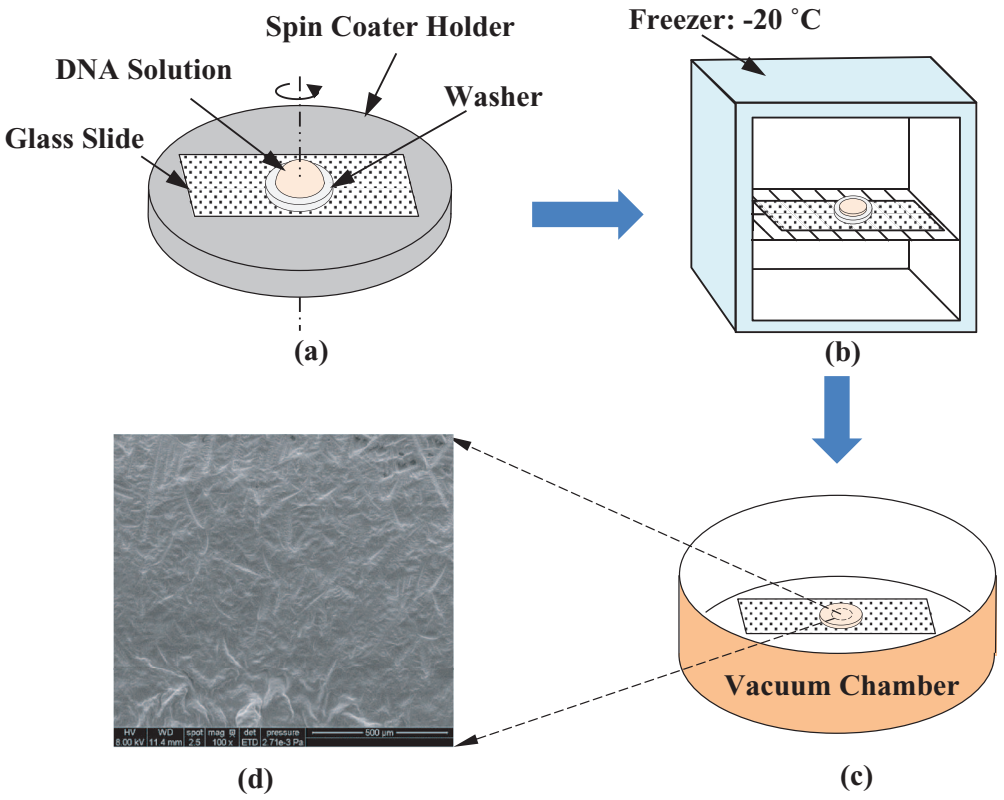

FIG. 2. Fabrication of uniform DNA-composited films: (a) the solution is dropped inside a washer taped to a microscope slide, and then the slide with the solution is spun in a spin coater to make the droplet uniform in the lateral direction; (b) the droplet is then frozen in a freezer (-20°C) for 1 hour, and the washer is then taken off; (c) the moisture in the composite is removed through the process of sublimation by placing the sample in a vacuum chamber down to 100 mTorr for another hour. (d) SEM image of part of the top surface of the composited film formed from DNA-TE buffer solution with 0.5 wt% DNA and 5 wt% NaCl.

of the film. At present, we still cannot form films with a pre-determined thickness. The average thickness of the measured film region is characterized by using a profilometer (Zygo NewView 7100).

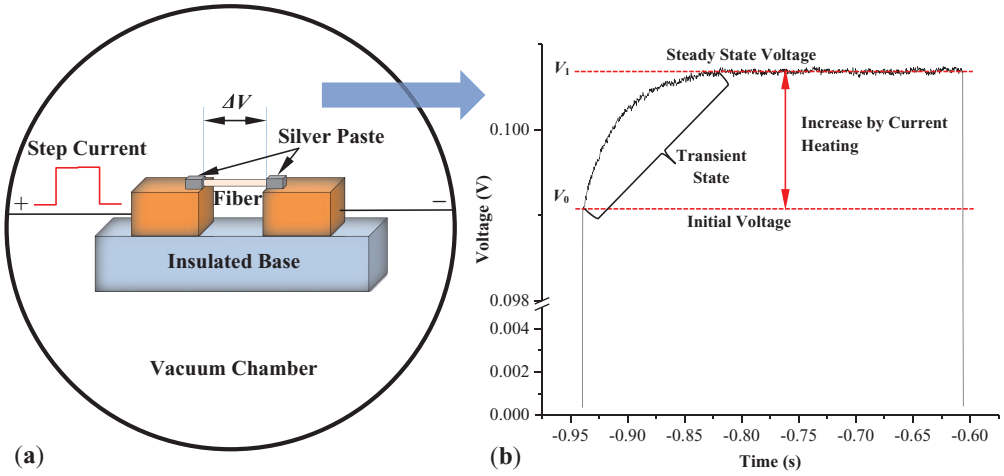

FIG. 3. (a) Schematic of the experimental principle of the TET technique to characterize the thermal diffusivity of DNA-composited fiber. (b) A typical *V-t* profile induced by the step DC current (recorded from the oscilloscope).

B. Characterization of thermal transport in DNA fibers

The thermal diffusivities of DNA-composited fibers can be measured by using the transient electro-thermal (TET) technique developed in our laboratory.[22] The effectiveness of this technique has been thoroughly confirmed by measuring the thermal diffusivities of conductive, semi-conductive and even non-conductive solid materials.[22–24] By using TET technique, Guo *et al.*[22] measured the thermal diffusivity of Pt wire to be $2.53 \sim 2.78 \times 10^{-5}$ m^2/s, close to the literature value of 2.51×10^{-5} m^2/s. Lin *et al.*[24] conducted TET experiments to measure the thermal diffusivity of insulated glass fiber to be 6.35×10^{-7} m^2/s, giving a thermal conductivity of 0.98 W/m · K with the effect of air cavity inside. The intrinsic thermal conductivity of glass is determined at 1.24 W/m · K, just slightly smaller than the thermal conductivity of bulk glass (1.38 W/m · K). The difference is caused by the extra cavity-induced phonon scattering in the microscale glass fiber. The experimental principle of the TET technique is shown in Fig. 3(a). During the experiment, a periodic step DC current is fed through the sample suspended between two electrodes to introduce joule heating. For the non-conductive DNA-composited fiber, a thin gold film is sputtering coated (DESK V, Denton Vacuum) on the top side of the fiber to make it electrically conductive. The transient temperature increase of the fiber due to joule heating is strongly dependent on its thermal diffusivity. The temperature increase leads to an electrical resistance increase, which then induces an overall voltage increase along the fiber. The temperature increase can be monitored through recording the voltage increase by a digital oscilloscope (DPO 3052, Tektronix). A typical voltage-time (*V-t*) profile is presented in Fig. 3(b). During the heating process, the voltage will increase from V_0 and reach the steady state V_1 via a transient state. The transient phase can be used to determine the thermal diffusivity of the DNA-composited fiber.

The physical model of the TET technique is simplified into a 1-D heat transfer model. The governing equation is

$$\frac{\partial(\rho c_p T)}{\partial t} = k\frac{\partial^2 T}{\partial x^2} + q_0 - 4\varepsilon_r \sigma\left(T^4 - T_0^4\right)/D, \tag{1}$$

where ρc_p and k are the heat capacity and thermal conductivity of the sample, respectively. D is the sample's average diameter. In the measurement, the sample can be considered as uniform enough if there is no bottleneck for the energy transport along the fiber length direction. Thus, we can use 1-D heat transfer model to describe the energy transport in the fiber sample. As shown in our results, no bottleneck is observed. For a specific sample, the diameter is measured $10 \sim 20$ times at different points along the fiber to achieve a small uncertainty in its measurement. q_0 is the electrical heating power per unit volume. $\sigma = 5.67 \times 10^{-8}$ W/m^{2}K^4 is the Stefan-Boltzmann constant, and ε_r is the

surface emissivity of the coated sample. The emissivity of the half coated gold is 0.02 ∼ 0.03, and the uncoated half is ∼0.9 for biomaterials. Thus the overall emissivity (ε_r) is estimated as 0.45.

To eliminate heat convection, the gold-coated fiber is measured in a vacuum chamber whose pressure is 1 ∼ 3 mTorr (detected by a convection vacuum gauge, CVM211 Stinger, InstruTech). In addition, the fiber ends are attached to copper electrodes by using silver paste to enhance the thermal and electrical conduction between them. In our work, the 2-probe method was used in the measurements. In general, the electrical contact resistance is only a few ohms, relatively small compared with the sample resistance (several hundred to several thousand ohms). The thermal contact resistance per unit area is around $10^{-7} \sim 10^{-8}$ m^{2}K/W for sound mechanical contact. For first order estimate, we can assume the thermal contact area is the product of the contact length and the circumference of the sample cross section embedded in the silver paste, which is around 10^{-9} m^2. So the thermal contact resistance is estimated to be around 100 K/W, negligible to the sample's thermal resistance ($10^7 \sim 10^8$ K/W). In addition, in Ref. 24, Lin has used the TET technique to measure the thermal diffusivity/conductivity of glass fibers close to the bulk values, indicating that the thermal contact resistance in the TET technique is negligible. The electrical heating power is assumed constant in the theoretical model. However, the electrical heating power will increase as the electrical resistance increases. The heating power is controlled in the experiment by selecting an appropriate loading current to have an electrical resistance increase no more than 2%.

By introducing $\theta = T - T_0$, and for most cases we have $\theta \ll T_0$, the radiation term in Eq. (1) can be expressed as $16\varepsilon_r \sigma T_0^3 \theta / D$. The normalized temperature increase $T^*(t)$, defined as $[T(t) - T_0] / [T(t \to \infty) - T_0]$, can be written as

$$T^* = \frac{96}{\pi^4} \sum_{m=1}^{\infty} \frac{1 - \exp[-(2m-1)^2 \pi^2 \alpha_{real+rad+gold} t / L^2]}{(2m-1)^4}, \tag{2}$$

where

$$\alpha_{real+rad+gold} = \alpha_{real} + \frac{L_{Lorenz} T L}{R A \rho c_p} + \frac{16 \varepsilon_r \sigma T_0^3}{(\rho c_p)_{real+gold}} D \frac{L^2}{\pi^2}. \tag{3}$$

The theoretical prediction T^* shown in Eq. (2) shares the same expression as the normalized voltage increase V^*, which is calculated as $[V(t) - V_0] / [V(t \to \infty) - V_0]$. Note that T^* (V^*) can be only shaped by different values of effective thermal diffusivity ($\alpha_{real+rad+gold}$) with known fiber length L, and then compared with the experimentally normalized voltage evolution. The value of $\alpha_{real+rad+gold}$, which gives the best fit of the experimental results by the least square method, will be taken as the effective thermal diffusivity of the sample. It includes the effect of gold and radiation.

The second term on the right hand side of Eq. (3) is referred as the "gold effect". R is the electrical resistance of the gold-coated fiber, and A the cross-sectional area of the bare fiber. The heat capacity (ρc_p) of the bare fiber is measured by the photothermal measurement of the DNA-composited film formed from the same solution. Since the fiber and the film are from the same solution, these two materials can be treated to share the same value of ρc_p. For the Lorenz number (L_{Lorenz}), the bulk value 2.45×10^{-8} WΩK^{-2} for gold at room temperature is not used in this work. We have checked the Lorenz number of gold film (20 ∼ 60 nm) by using spider silk fiber samples (Nephila Clavipes and Western Black Widow). Briefly, the same spider silk fiber sample is coated with gold twice, and the TET technique is applied twice to characterize its thermal diffusivities. For each coating, we can measure $\alpha_{real+rad+gold}$ and R for the gold-coated sample. The last term in Eq. (3) can be treated as the "radiation effect", which is a constant for two coatings on the same sample. Finally we solve for the unknowns which are α_{real} and L_{Lorenz}. The Lorenz number of the gold film is measured to be 2.27×10^{-8} WΩK^{-2}, which is fairly close to the bulk value.

C. Characterization of thermal transport in DNA films

The thermophysical properties of DNA-composited films are measured by using the noncontact photothermal technique.[25–27] Using this technique, Wang *et al.*[27] obtained the thermal conductivity of polymethyl methacrylate (PMMA) film at 0.149 W/m · K, which is consistent with bulk values.

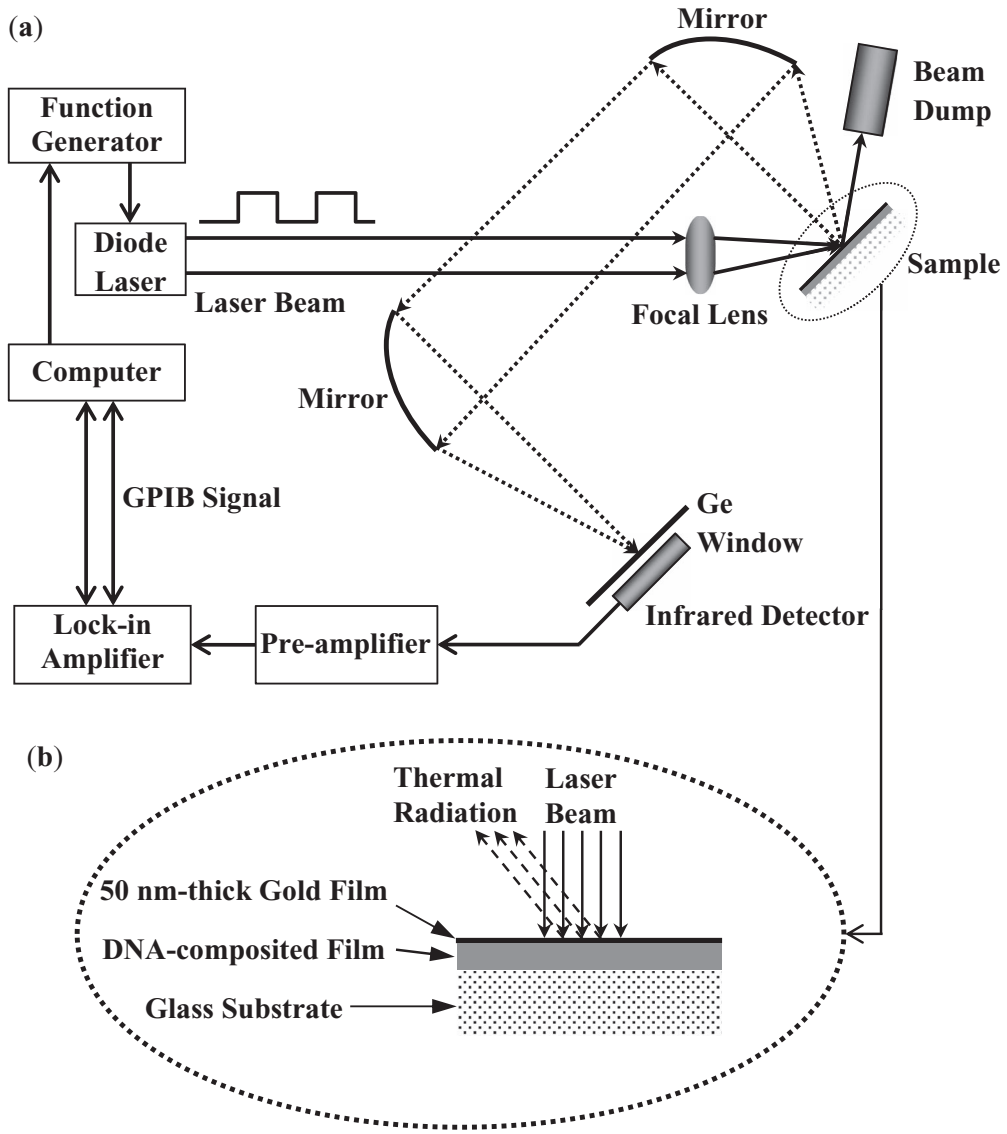

FIG. 4. (a) A schematic of the experimental setup for the photothermal technique and (b) the structure of the DNA-composited film sample.

This measurement is also intended to provide the data of ρc_p that can be used to process the DNA-composited fiber result to obtain its thermal diffusivity and conductivity. A schematic of the photothermal technique is shown in Fig. 4. In the experiment, a continuous infrared diode laser (BWTEK BWF-2, 809 nm wavelength) modulated by a function generator is directed and focused on the film to induce direct heating and periodic temperature variation at the film surface. To have the laser beam absorbed on the surface in a controlled way, a 50 nm-thick gold film is sputtering coated (DESK V, Denton Vacuum) on top of the film. The temperature variation due to laser heating is strongly dependent on the thermophysical properties of the film. When the temperature variation is not very large, it has a linear relationship with the change of the thermal radiation as $\Delta E \propto \varepsilon\sigma T_0^3 \Delta T$, where ε is the surface emissivity and T_0 the initial surface temperature. Therefore, the temperature variation can be sensed by measuring the thermal radiation from the film surface, which is directed to an infrared detector. In order to filter out the reflected laser beam, a Ge window is placed in front of the detector to allow only the thermal radiation to pass. The signal from the infrared detector is

pre-amplified and then measured by a lock-in amplifier. The experiment is controlled by a computer for automatic data acquisition.

In particular, the phase shift (ϕ) between the thermal radiation and the modulated laser beam is used to determine the thermophysical properties of the DNA-composited film in this experiment. The system will inevitably introduce a phase shift (ϕ_{cal}) by itself, which can be calibrated by measuring the reflected laser beam from the sample. In the experiment, the modulation frequency is set between 17 Hz and 20 kHz. The spot of the laser beam is about 0.7 mm × 1.4 mm (the beam is not perpendicular to the sample surface), which is larger than the thermal diffusion depth in the lateral direction of the sample within the frequency range. As a result, the thermal transport induced by laser heating can be treated as one-dimensional along the thickness direction of the film. Theoretical descriptions between the phase shift and thermophysical properties of the to-be-measured film have been developed and detailed in our past work.[25]

After the experiment, trial values of unknown properties such as thermal diffusivity/conductivity and interface resistance will be used to calculate the theoretical phase shift and compare it with the measured phase shift at each frequency. The trial values giving the best fit of the experimental results (the least square method) will be taken as the properties of the sample.

III. Results and discussion

A. Thermal transport in DNA-composited fibers

For the microscale DNA-composited fibers with roughly 40 nm-thick gold coating, there are no coherent quantum tunneling and diffusive thermal hopping due to the relatively large-scale electrical transport. As a result, there is no non-linear effect in the electrical signal as we checked, which occurs, by contrast, in DNA-gold composite.[17] We have confirmed that the *I-V* of our gold-coated DNA-composited fiber is linear, which is important for appropriately applying the TET technique.

The composites are divided into two groups: Group 1, containing fibers and films from the solution with 0.5 wt% DNA and 5 wt% NaCl, and the composites in Group 2, from the solution with 1 wt% DNA and 1 wt% NaCl. There are 8 and 5 fibers with different lengths and diameters in Group 1 and Group 2, respectively. Note that although we cannot fully control the length and diameter of a fiber, the size effects are addressed in the gold and radiation effects, which are subtracted in the data processing. Therefore, the real thermal diffusivity/conductivity will be independent of the fiber size from the measurement aspect. Figure 5(a) shows the comparison between the theoretical fitting results and the experimental normalized temperature rise for the fibers. The uncertainty of the fitting process is also illustrated in Fig. 5(a) by plotting another two fitting curves with ± 10% variation of the effective thermal diffusivity ($\alpha_{real+rad+gold}$). It is conclusive that the percentage uncertainty of the fitting process is below 10%. Due to multiple measurements, the average result of $\alpha_{real+rad+gold}$ can have an uncertainty even smaller (∼2%). The average value of $\alpha_{real+rad+gold}$ for each fiber is taken as the experimental result shown in Table I with its uncertainty. Then the gold and radiation effects are subtracted to obtain the real thermal diffusivity (α_{real}). To do this, the heat capacity (ρc_p) of the fiber is required. From the photothermal characterization of the films, the average values of ρc_p are determined as 1.25×10^6 J/m^{3}K and 1.21×10^6 J/m^{3}K for the fibers in each group. At last, the real thermal conductivity is calculated according to the expression $k = \alpha \rho c_p$.

B. Thermal transport in DNA-composited films

There are 4 and 3 DNA-composited films with different film thickness measured by using the photothermal technique in two groups. The importance of film thickness (L) on thermal transport is two-fold. On one hand, two main parameters are determined by the data fitting: L/k, and $L\rho c_p$. Thus, the thermal conductivity and heat capacity is directly dependent on the thickness measurement accuracy. The uncertainty of the film thickness is shown in Table II to evaluate the accuracy of thickness measurement. In addition, thermal effusivity defined as $\sqrt{k\rho c_p}$ is a parameter independent of the film thickness in the photothermal technique, which can be compared between two group films. On the other hand, film structure can vary

TABLE II. Experimental data and calculated results for all DNA composited-films.

Films	L (μm)	ρc_p ($\times 10^6$J/m^{3}K)	k (W/m $\cdot$ K)	$\sqrt{k\rho c_p}$ ($\times 10^3$J/m^{2}Ks$^{0.5}$)	α (10^{-6}m^2/s)	R_{tc} (m^{2}K/W)
Group 1_1	36.21 ± 0.17	1.244 ± 0.126	7.40 ± 0.75	3.072	6.00 ± 0.85	1.0×10^{-9}
Group 1_2	38.13 ± 0.17	1.631 ± 0.163	15.53 ± 1.56	5.033	9.52 ± 1.35	1.0×10^{-9}
Group 1_3	13.37 ± 0.20	1.011 ± 0.102	20.69 ± 2.09	4.574	20.46 ± 2.93	1.3×10^{-7}
Group 1_4	26.85 ± 0.41	1.108 ± 0.112	12.40 ± 1.25	3.707	11.19 ± 1.60	1.0×10^{-9}
Group 2_1	23.65 ± 0.30	0.993 ± 0.100	3.65 ± 0.37	1.904	3.67 ± 0.52	8.9×10^{-6}
Group 2_2	36.03 ± 0.54	1.094 ± 0.111	3.29 ± 0.33	1.896	3.00 ± 0.43	4.4×10^{-5}
Group 2_3	22.62 ± 0.31	1.556 ± 0.157	2.05 ± 0.21	1.786	1.32 ± 0.19	5.4×10^{-5}

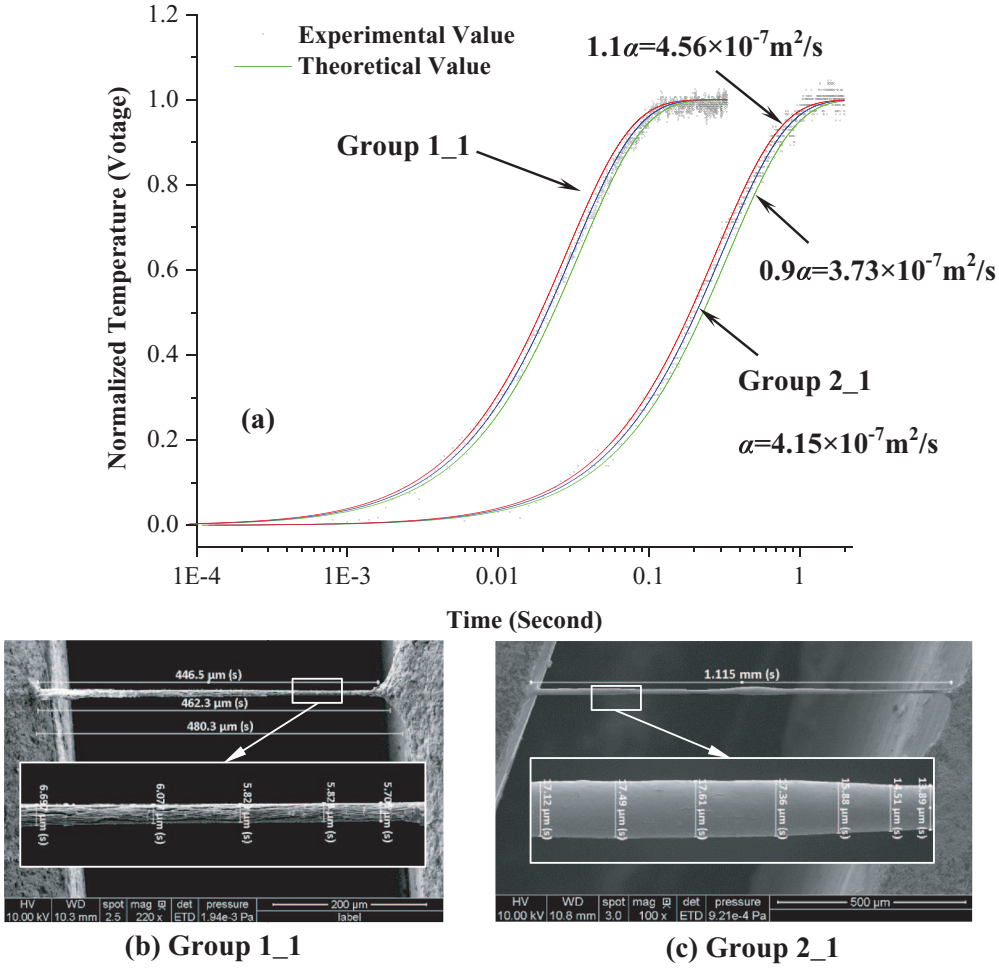

FIG. 5. (a) TET fitting results for DNA fibers: the experimental normalized temperature rise versus time, theoretical fitting results, and another two fitting curves with $\pm$ 10% variation of $\alpha_{real+rad+gold}$ to demonstrate the uncertainty of the fitting process (Red lines are for $+10\%$, and green lines are for -10%). (b) $\sim$ (c) SEM images of the fibers in the two groups.

with film thickness. It is expected that a thicker film is much easier to have pore structures inside. This effect can be evaluated by the thermal contact resistance between the film and the glass substrate.

Figure 6(a) shows the phase shift fitting results against the experimental data for one film in Group 1. The data fitting determines the thermal conductivity and heat capacity with the

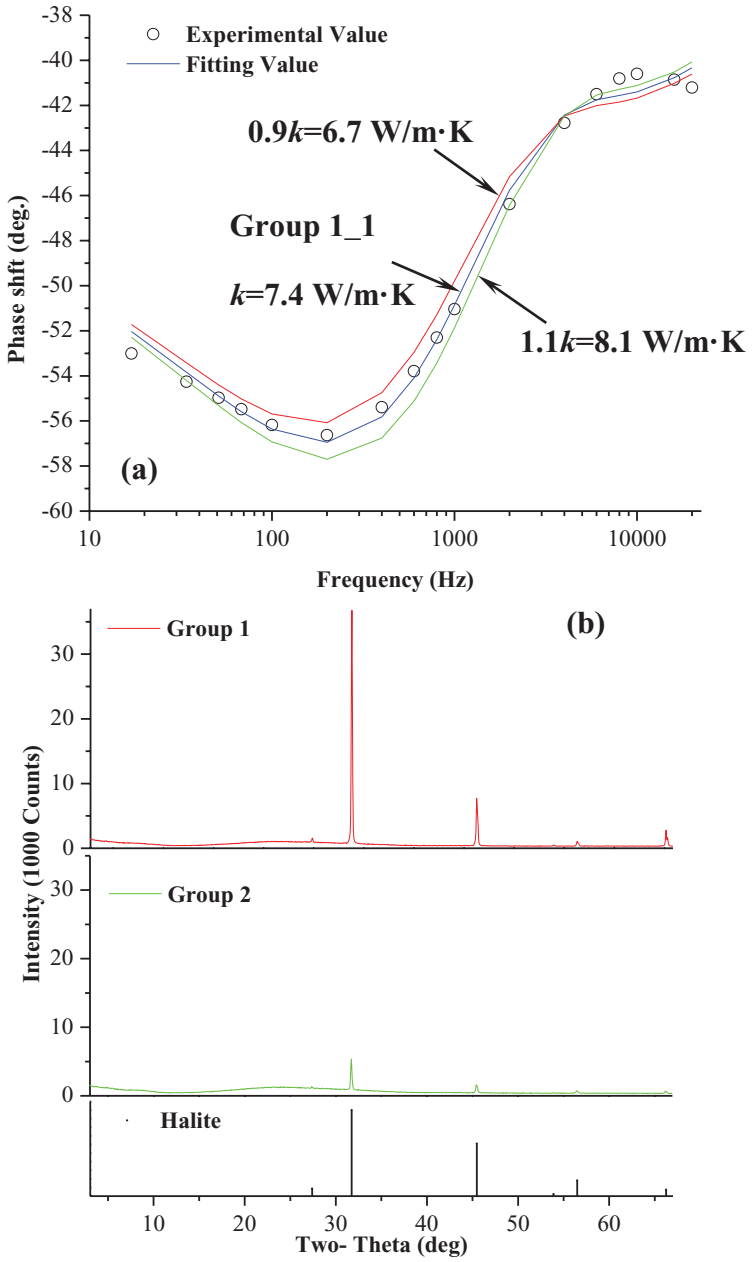

FIG. 6. (a) Data fitting of the phase shift for the film of Group 1_1 (symbol is for experimental data, and solid lines are theoretical fitting). Another two fitting curves with ± 10% variation of thermal conductivity (k) are plotted to show the uncertainty of the fitting (Red line is for −10%, and green line is for + 10%). (b) x-ray Diffraction patterns of the DNA-composited films in two groups. The bottom one is the XRD pattern of Halite-NaCl for comparison.[28]

film thickness. To evaluate the uncertainty of the fitting process, two fitting curves with ± 10% variation of the thermal conductivity with other fixed parameters are plotted. This shows that the percentage uncertainty of the fitting is not more than 10%. We then use 10% for the uncertainty for the fitting process and the uncertainty of the thickness to estimate the uncertainty of thermal conductivity and heat capacity. The thermal contact resistance (R_{tc}) at the glass substrate/film interface is also given. All results for the DNA-composited films are listed in Table II.

C. Structure and physics behind the measurement results

The top and center of Fig. 6(b) show the x-ray Diffraction (XRD) patterns of the DNA-composited films in the two groups. The scans are collected using the same parameters (a step size of 0.05 degrees and a dwell time of 3 seconds). The bottom of the figure is the reference XRD pattern of Halite-NaCl for comparison.[28] A profile fitting is used to determine precise peak positions and to estimate the crystallite size. The fitting results show that all peaks in both measured diffractograms match the reference Halite-NaCl pattern. Meanwhile, the peaks in both diffractograms are too narrow to give reliable crystallite size estimates (larger than 100 nm), which indicates both films contain NaCl crystals with a large crystallite size. The film in Group 2 in XRD study is about 20 μm thick while the one of Group 1 for XRD study is about 10 μm thick. The NaCl concentration in the Group 1 film is about two times that of the Group 2 film. Thus we expect both films will give similar peak height in XRD study. However, Fig. 6 shows the Group 2 film has a much lower peak intensity that the Group 1 film, indicating this film contains less NaCl crystals. To check the effect of NaCl in the composites, its thermal properties are summarized. The density of NaCl is 2.17×10^3 kg/m^3, and its specific heat at 300 K is 859.2 J/kgK.[29] So the heat capacity of NaCl is 1.86×10^6 J/m^{3}K. The thermal conductivity of NaCl at 323 K is 5.6 W/m $\cdot$ K,[29] therefore, its thermal diffusivity is 3.0×10^{-6} m^2/s.

First we compare the results of fibers in the two groups. The average thermal diffusivity and thermal conductivity of fibers in Group 1 is 3.86×10^{-7}m^2/s and 0.63 W/m $\cdot$ K, respectively, which are both larger than those of the fibers in Group 2 (1.92×10^{-7}m^2/s and 0.33 W/m $\cdot$ K). F-test shows that the difference between these two groups is statistically significant. From the SEM images of the fibers in both groups, it is observed that all fibers in Group 1 have evident and visible aligned fiber structure, while the fibers in Group 2 do not [Fig. 5(b) $\sim$ 5(c)]. Excluding the effect of fiber size, we conclude that the enhancement of thermal transport is due to the DNA structure alignment. In the initial solution, NaCl is speculated to have an effect on regulating the structure of DNA. Adding NaCl into the buffer will generate a charge "screening" effect: Na^+ ions will "screen" some of the negative charges of the phosphate groups (PO_4^{3-}) in the backbone. This effect will align the DNA molecules with the NaCl crystal structures during crystallization, which will enhance the thermal transport within the composite.

Similarly, films in Group 1 have a larger thermal diffusivity and thermal conductivity than those of the films in Group 2 considering the inaccuracy of thickness measurement. Group 1 films also have a larger thermal effussivity. The depression of thermal conduction in Group 2 films is mainly ascribed to the pore structure. Although the regions without large crystals examined by naked eyes are chosen to measure, pore structure still cannot be excluded from the film with the current film fabrication technique. This conclusion is confirmed by the thermal contact resistance at the glass substrate/film interface. The thermal contact resistance is quite small for the Group 1 films (with the largest one at 1.3×10^{-7} m^{2}K/W), much smaller than the thermal resistance of the film (1.5×10^{-6} m^{2}K/W). This indicates that the films in this group have less and even negligible pore structure. In contrast, the average thermal contact resistance for the Group 2 films is around 3.6×10^{-5} m^{2}K/W. A large thermal contact resistance indicates that the pore structure is filled with air formed inside the film. Besides, the most impressive result is that the thermal conductivity and thermal diffusivity of films in Group 1 are higher than those of NaCl, even though their heat capacities are similar. This result again suggests that DNA molecules are aligned with the NaCl crystal structure during crystallization, which resulted in a significant enhancement of thermal transport within the composites, both in fibers and films.

In the last, the thermal conductivity and diffusivity of the fibers in both groups are much lower than those of the films of the same group. We note that the fibers and films should have different structures due to different sample preparation method and condition. Fibers are drawing in room temperature without any solidification control, while the films are first frozen to a low temperature and then placed in a vacuum to allow for controlled sublimation. We expect the fast solidification during fiber synthesis will lead to less-ordered structure. Different structure will lead to different thermal transport capacity. In addition, heat is mainly conducted through fiber structure without NaCl since NaCl crystals are only discretely distributed on the fiber surface, as shown in Fig. 5(b)

and 5(c). In contrast, heat is conducted through the film structure with NaCl in a film. Hence, NaCl will make more contributions in thermal transport in a film than a fiber.

IV. CONCLUSION

In this work, crystalline DNA composite films and micro-fibers were synthesized, and their thermal transport capacity was characterized for the first time. The DNA-composited fibers and films were formed from two groups of solutions: Group 1 is 0.5 wt% DNA with 5 wt% NaCl, and Group 2 is 1 wt% DNA with 1 wt% NaCl. Large amount of bond of Na^+ ion and phosphate group in the solution was speculated to align the DNA molecule with the NaCl crystal structure during crystallization, which resulted in a significant enhancement of thermal transport within the composites, including the fibers and films. The discrepancy of the thermal conductivity/diffusivity of the fibers and films was due to the sample-to-sample structure variation and directions of thermal transport with respect to the distribution of NaCl. The DNA composite films were found to have a higher capacity of thermal transport than DNA composite microfibers, largely due to the slow and controlled solidification in film formation that favors formation of more ordered structure.

ACKNOWLEDGMENT

Support of this work from the Army Research Office (W911NF-12-1-0272) and Office of Naval Research (N000141210603) is gratefully acknowledged. We thank Christopher Reilly very much for proofreading the manuscript. X.W thanks the support of the "Taishan Scholar" program of Shandong Province, China.

[1] C. A. Mirkin, R. L. Letsinger, R. C. Mucic, and J. J. Storhoff, Nature **382**, 607 (1996).
[2] A. P. Alivisatos, K. P. Johnsson, X. G. Peng, T. E. Wilson, C. J. Loweth, M. P. Bruchez, and P. G. Schultz, Nature **382**, 609 (1996).
[3] E. Braun, Y. Eichen, U. Sivan, and G. Ben-Yoseph, Nature **391**, 775 (1998).
[4] D. D. Eley and D. I. Spivey, Transactions of the Faraday Society **58**, 411 (1962).
[5] P. J. Dandliker, R. E. Holmlin, and J. K. Barton, Science **275**, 1465 (1997).
[6] C. Dekker and M. A. Ratner, Physics World **14**, 29 (2001).
[7] F. D. Lewis, T. F. Wu, Y. F. Zhang, R. L. Letsinger, S. R. Greenfield, and M. R. Wasielewski, Science **277**, 673 (1997).
[8] M. Bixon, B. Giese, S. Wessely, T. Langenbacher, M. E. Michel-Beyerle, and J. Jortner, Proceedings of the National Academy of Sciences of the United States of America **96**, 11713 (1999).
[9] Y. A. Berlin, A. L. Burin, and M. A. Ratner, Journal of the American Chemical Society **123**, 260 (2001).
[10] B. Giese, J. Amaudrut, A. K. Kohler, M. Spormann, and S. Wessely, Nature **412**, 318 (2001).
[11] H. W. Fink and C. Schonenberger, Nature **398**, 407 (1999).
[12] L. T. Cai, H. Tabata, and T. Kawai, Applied Physics Letters **77**, 3105 (2000).
[13] P. J. de Pablo, F. Moreno-Herrero, J. Colchero, J. Gomez-Herrero, P. Herrero, A. M. Baro, P. Ordejon, J. M. Soler, and E. Artacho, Physical Review Letters **85**, 4992 (2000).
[14] D. Porath, A. Bezryadin, S. de Vries, and C. Dekker, Nature **403**, 635 (2000).
[15] A. Y. Kasumov, M. Kociak, S. Gueron, B. Reulet, V. T. Volkov, D. V. Klinov, and H. Bouchiat, Science **291**, 280 (2001).
[16] A. J. Storm, J. van Noort, S. de Vries, and C. Dekker, Applied Physics Letters **79**, 3881 (2001).
[17] T. Kodama, A. Jain, and K. E. Goodson, Nano Letters **9**, 2005 (2009).
[18] C. Kittel, *Introduction to solid state physics*, 8th ed. (J. Wiley, Hoboken, NJ, 2005).
[19] K. A. Velizhanin, C. C. Chien, Y. Dubi, and M. Zwolak, Physical Review E **83**, 050906 (2011).
[20] A. V. Savin, M. A. Mazo, I. P. Kikot, L. I. Manevitch, and A. V. Onufriev, Physical Review B **83**, 245406 (2011).
[21] S. A. Harfenist, S. D. Cambron, E. W. Nelson, S. M. Berry, A. W. Isham, M. M. Crain, K. M. Walsh, R. S. Keynton, and R. W. Cohn, Nano Letters **4**, 1931 (2004).
[22] J. Q. Guo, X. W. Wang, and T. Wang, Journal of Applied Physics **101**, 063537 (2007).
[23] X. H. Feng, X. P. Huang, and X. W. Wang, Nanotechnology **23**, 185701 (2012).
[24] H. Lin, S. Xu, X. Wang, and N. Mei, Small **9**, 2585 (2013).
[25] X. W. Wang, H. P. Hu, and X. F. Xu, Journal of Heat Transfer-Transactions of the Asme **123**, 138 (2001).
[26] X. W. Wang, Z. R. Zhong, and J. Xu, Journal of Applied Physics **97**, 064302 (2005).
[27] T. Wang, X. W. Wang, Y. W. Zhang, L. Y. Liu, L. Xu, Y. Liu, L. J. Zhang, Z. Y. Luo, and K. F. Cen, Journal of Applied Physics **104**, 013528 (2008).
[28] R. T. Downs, K. L. Bartelmehs, G. V. Gibbs, and M. B. Boisen, American Mineralogist **78**, 1104 (1993).
[29] Chemical Rubber Company., *Handbook of chemistry and physics* (CRC Press, Cleveland, Ohio, 2004).